Phase-Unsynchronized Power Decoupling Control of MMC Based on Feedback Linearization

Yuntao Zou, *Student Member, IEEE*, Lei Zhang, *Member, IEEE*, Jiangchao Qin, *Senior Member, IEEE*, Wanxing Sheng, *Senior Member, IEEE*, and Qing Duan, *Member, IEEE*

***Abstract*—The traditional power decoupling control of modular multilevel converter (MMC) is based on the phase synchronization achieved by the phase-locked loop (PLL), and MMC intricate inner dynamics are ignored, which jeopardizes the system stability and power decoupling. To improve the performance, a nonlinear phase-unsynchronized power decoupling control for MMC is proposed without PLL. At first, the MMC model as a nonlinear multi-input multi-output system is developed. The developed model illustrates that the MMC power coupling is caused by the ac current as well as the MMC capacitor voltages. Then, through the input–output linearization method, the proposed method decouples the MMC output powers without the phase synchronization. Involving integral control, the dynamics of MMC output powers are designed as second-order systems so that the control parameters can be easily determined based on the required transient performance. To verify the accuracy and correctness of the developed model, a comparison of MMC dynamics with the proposed control is conducted between the numerical solution in MATLAB and the EMT simulation in PSCAD/EMTDC. Moreover, seven cases in the EMT simulations and four cases in the experimental results demonstrate the desired phase asynchronization and power decoupling performance of the proposed method compared with the conventional *dq* control. At last, the system zero dynamic stability is investigated and the influences of MMC control parameters, ac-side voltage, dc-side voltage and equilibrium points are analyzed to evaluate the stability performance of the proposed method.**

***Index Terms*—Feedback linearization, modular multilevel converter (MMC), nonlinear system, phase asynchronization, phase-locked loop (PLL), power decoupling.**

I. Introduction

MODULAR multilevel converter (MMC) is the most attractive topology in the modern ac/dc hybrid power system for the bulk power transmission and the gird-connection of renewable energy sources due to its adaptive high-voltage application, strong reliability, and flexible scalability [1]–[3]. The cascaded control based on the synchronous reference frame, i.e., *dq* control, is widely applied. Meanwhile, the power decoupling is performed in the *dq* control through the phase synchronization with the phase-locked loop (PLL). Thus, the *dq* control has become the most fundamental control scenario of MMCs for the applications, e.g., the dc-grid voltage balancing and the fast ac-grid frequency support [4], [5].

However, two critical problems of the conventional *dq* control need to be considered. The first problem is that, when the conventional *dq* control for two-level voltage source converters (VSCs) is applied to the MMC, it does not consider the internal dynamics of MMC [1], [6], which makes it difficult to realize the MMC power decoupling accurately [1]. Furthermore, the imprecise power decoupling caused by the conventional *dq* control will also bring unnecessary system transients that are harmful to the power quality [1], [7].

The second problem is that the PLL can make the system stability more vulnerable. In recent years, the instabilities caused by the PLL in the grid-integrations of two-level VSCs are reported and discussed. Zhou *et al.* [8]–[11] indicate that, an ac power grid with high impedance, i.e., the weak grid, has a strong coupling with the nonlinear dynamics of the high bandwidth PLL, which leads to a potential instability. Hence, the performance of *dq* control is constrained by the short-circuit ratio of ac power grids.

Several control methods are proposed considering the influence of MMC inner dynamics on the power decoupling performance. Wang *et al.* [12]–[14] improve the conventional *dq* control by employing the feedforward control to compensate the dynamics of the capacitor voltages. The feedback linearization technique, as a powerful tool to sharp the plant dynamic through state feedbacks [15], has been widely applied to the high-dimensional and nonlinear system, e.g., the VSC-based driver controls for permanent magnet synchronous generator [16], doubly fed induction generator [17], and induction motor [18]. Meanwhile, this technique can be utilized for VSC control, e.g., dc voltage control [19]. Due to the high-dimensional and nonlinear features of MMC, Yang *et al.* [20] and Li *et al.* [21] develop the *dq* currents decoupling control laws based on the input–output linearization instead of the conventional two power control loops. Although the methods aforementioned consider the influence of the MMC inner dynamics on the control performance, the power decoupling principle of these methods is still based on the phase-synchronization achieved by PLL.

On the other side, many previous works have discussed the controls for VSC without PLL. Gui *et al.* [22]–[24] express the

Manuscript received March 12, 2021; revised May 30, 2021, July 29, 2021, and August 30, 2021; accepted October 3, 2021. Date of publication October 14, 2021; date of current version November 30, 2021. Recommended for publication by Associate Editor S. Golestan. *(Corresponding author: Jiangchao Qin.)*

Yuntao Zou and Lei Zhang are with the School of Electrical, Computer, and Energy Engineering, Arizona State University, Tempe, AZ 85287-5706 USA (e-mail: yzou46@asu.edu; zhanglei19891025@gmail.com).

Jiangchao Qin is with the Department of Electrical Engineering, Shanghai Jiao Tong University, Shanghai 200240, China (e-mail: jqin@asu.edu).

Wanxing Sheng and Qing Duan are with the Beijing Key Laboratory of Distribution Transform, China Electric Power Research Institute, Beijing 100192, China (e-mail: wxsheng@epri.sgcc.com.cn; duanqing@epri.sgcc.com.cn).

Color versions of one or more figures in this article are available at https://doi.org/10.1109/TPEL.2021.3119527.

Digital Object Identifier 10.1109/TPEL.2021.3119527

control methods based on the VSC using instantaneous power in the stationary reference frame without PLL. However, the feedback variables in the stationary reference frame must be fundamental frequency sinusoidal functions where they need a non-distorted grid voltage [22]. Thus, filters are introduced in the control loops which jeopardize the power decoupling. In addition, Zhong *et al.* [25] and [26], the virtual synchronous generator (VSG) control generates the magnitude and phase of modulation references based on the model of synchronous generator. Since the generation of modulation references only depends on the control itself, it can be applied to different converters, e.g., two-level VSC and MMC. However, the VSG control has no capability to achieve the power decoupling while the influences of converter dynamics are ignored. The power synchronization control [27] uses the rotor kinetic equation to generate the phase information instead of the PLL, which employs the advantage of the VSG control. However, the damping of this control is quite low when applied to the weak grid. On the other side, the power dynamics of these methods are complicated, and hence the associated control parameters are difficult to determine. In sum, the existing methods are mostly based on the two-level VSC model or MMC average value model, which cannot achieve a completed power decoupling.

Therefore, to obtain the accurate decoupling power control, the MMC inner dynamics should be considered. It is also expected that the stability may be improved by eliminating the PLL. Therefore, in this article, a control method is proposed for MMC power control based on the input–output linearization technique. The accurate MMC model is established in the *dq* reference frame with arbitrary initial phase angle to reflect the inner dynamics of voltages and currents of the dc, fundamental-frequency, and second-order harmonic components. Then, a phase-unsynchronized power decoupling control of the MMC is proposed without PLL. The purposes of the proposed method are emphasized as compensating MMC inner dynamics, eliminating PLL, guaranteeing power decoupling, and having better power dynamics. For the weak grid application of the proposed method, it will be discussed in another article with more evaluation and investigation.

The contributions of this article are summarized as follows.

1) Unlike the VSG control, the proposed control still maintains power decoupled without introducing the PLL, i.e., the phase-unsynchronized condition, as its main advantage. Furthermore, the MMC power dynamic is designed as a second-order system, which is convenient to determine the control parameters for adjusting the regulation speed, overshooting, damping feature, etc.
2) The proposed control considers the influence of MMC inner dynamics on the power control. Thus, a thorough and precise power decoupling can be achieved, which avoids unnecessary dynamic transients of the MMC inner side and the MMC-tied ac/dc power system.
3) A detailed investigation is performed for the stability of the system zero dynamic of the MMC with the proposed control. The associated results show that the stability of the proposed method is not affected by the control parameters and sensitive to the grid parameters of the MMC dc-side and point of common coupling (PCC) bus.

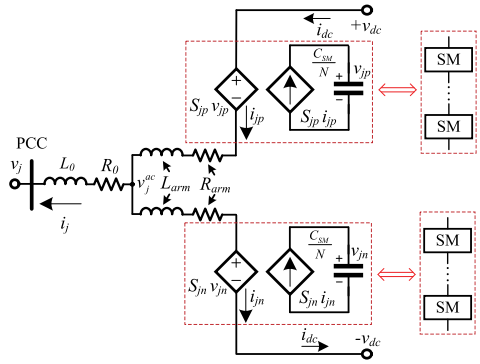

Fig. 1. Schematic of MMC arm switching function model for phase j.

II. State-Space Model of MMC

Fig. 1 exhibits the schematic of the MMC arm switching function model [28], [29] for phase j, where $j = a, b,$ and c. N is the number of submodules in each arm and C_{SM} is the capacitance of submodule. L_{arm} and L_0 are the inductances of each arm and PCC connection, respectively. R_{arm} and R_0 are the resistances of each arm and the PCC connection, respectively. The three-phase dynamics of the arm currents, arm voltages, ac-side currents, and switching functions are, respectively, given by

$$\begin{aligned} &v_{\text{dc}} - S_{jp}v_{jp} - R_{\text{arm}}i_{jp} - L_{\text{arm}}\frac{di_{jp}}{dt} = v_j^{\text{ac}} \\ &-v_{\text{dc}} + S_{jn}v_{jn} + R_{\text{arm}}i_{jn} + L_{\text{arm}}\frac{di_{jn}}{dt} = v_j^{\text{ac}} \end{aligned} \tag{1}$$

$$\frac{C_{SM}}{N}\frac{dv_{jp}}{dt} = S_{jp}i_{jp}, \quad \frac{C_{SM}}{N}\frac{dv_{jn}}{dt} = S_{jn}i_{jn} \tag{2}$$

$$v_j^{\text{ac}} = v_j + R_0 i_j + L_0\frac{di_j}{dt}, \tag{3}$$

$$S_{jp} = \frac{1}{2} - \frac{v_j^{\text{ref}}}{\tilde{V}_{\text{dc}}}, \qquad S_{jn} = 1 - S_{jp} = \frac{1}{2} + \frac{v_j^{\text{ref}}}{\tilde{V}_{\text{dc}}} \tag{4}$$

where v_{jp}, v_{jn}, i_{jp}, and i_{jn} are the equivalent capacitor voltages and the arm currents of upper and lower arms, respectively. v_j^{ac} and v_{dc} are the MMC ac-side and dc-side voltages, respectively. v_j is the phase j voltage of PCC bus. S_{jp} and S_{jn} are the switching functions of the upper and lower arms, respectively. $\tilde{V}_{\text{dc}}$ is the nominal dc voltage of MMC and v_j^{ref} is the phase j voltage reference generated by the controller.

In the dynamic behavior of MMC, the dc, fundamental-frequency, and second-order harmonic components are the dominated elements [30]. Therefore, the arm voltages and currents are exhibited as

$$\begin{aligned} &v_{jp} = v^{\text{dc}} + v_j^{\omega_0} + v_j^{2\omega_0}, \quad i_{jp} = \frac{1}{3}i_{\text{dc}} + \frac{1}{2}i_j + i_j^{2\omega_0} \\ &v_{jn} = v^{\text{dc}} - v_j^{\omega_0} + v_j^{2\omega_0}, \quad i_{jn} = \frac{1}{3}i_{\text{dc}} - \frac{1}{2}i_j + i_j^{2\omega_0} \end{aligned} \tag{5}$$

where v^{dc}, $v_j^{\omega_0}$, $v_j^{2\omega_0}$ and i_{dc}, i_j, $i_j^{2\omega_0}$ are the dc, fundamental frequency, and the second-order harmonic voltages and currents, respectively. Substituting (4) and (5) into (1), (2), and (3) while eliminating v_j^{ac}, the dynamics of MMC in the dq reference frame are given in Appendices (A1), (A2) and (A3). The corresponding coefficients $c_1, \ldots, c_8$ are expressed in (A4).

The active and reactive powers of PCC bus are expressed as

$$P = 1.5\left(v_d i_d + v_q i_q\right), \quad Q = 1.5\left(v_q i_d - v_d i_q\right). \tag{6}$$

Thus, based on (A2) and (6), the dynamics of the MMC active and reactive powers are related to the i_d, i_q, $v_d^{\omega_0}$, $v_q^{\omega_0}$, $v_d^{2\omega_0}$, $v_q^{2\omega_0}$, v_d^{ref}, and v_q^{ref}, which indicates that the dynamics of MMC SM capacitor voltage will significantly affect the MMC power decoupling. Hence, ignoring the MMC inner dynamics will negatively influence MMC control.

In sum, the ten-order nonlinear state-space model of MMC, as a two-input two-output system, is derived and shown in (7) by choosing the state variables as $\boldsymbol{x}^T = [i_{\text{dc}}, v^{\text{dc}}, i_d, i_q, v_d^{\omega_0}, v_q^{\omega_0}, i_d^{2\omega_0}, i_q^{2\omega_0}, v_d^{2\omega_0}, v_q^{2\omega_0}]$, the system inputs as $\boldsymbol{u}_1 = v_d^{\text{ref}}$, $\boldsymbol{u}_2 = v_q^{\text{ref}}$, and the system outputs as $\boldsymbol{y}_1 = h_1(\boldsymbol{x}) = P$, $\boldsymbol{y}_2 = h_2(\boldsymbol{x}) = Q$.

$$\begin{cases} \dot{\boldsymbol{x}} = \boldsymbol{f}(\boldsymbol{x}) + \boldsymbol{g}_1(\boldsymbol{x})\boldsymbol{u}_1 + \boldsymbol{g}_2(\boldsymbol{x})\boldsymbol{u}_2 \\ y_1 = h_1(\boldsymbol{x}) \\ y_2 = h_2(\boldsymbol{x}). \end{cases} \tag{7}$$

The dq transform matrices employed in this article for fundamental frequency and second-order harmonic components are given by

$$T_{abc/dq} = \frac{2}{3}\begin{bmatrix} \cos(\theta) & \cos(\theta - \frac{2}{3}\pi) & \cos(\theta + \frac{2}{3}\pi) \\ -\sin(\theta) & -\sin(\theta - \frac{2}{3}\pi) & -\sin(\theta + \frac{2}{3}\pi) \end{bmatrix} \tag{8}$$

where $\theta = \omega_0 t$ or $2\omega_0 t$.

According to (8), it is emphasized that there is no PLL utilized for phase synchronization. Hence, the power decoupling method of the proposed control in this article is different with the conventional synchronous rotating frame control, i.e., dq control, and the stationary reference frame control, i.e., $\alpha\beta$ control [4]. By employing the phase-unsynchronized *dq* transformation, the number of the state variables can be reduced.

III. Proposed Power Control of MMC

A. Input–Output Linearization Control for MIMO System

The basic background of the input–output linearization technique for the multi-input multi-output (MIMO) system [15], [31] is briefly introduced in this part. In particular, a square MIMO system, which has the equal number of inputs and outputs, is considered as

$$\begin{cases} \dot{\boldsymbol{x}} = \boldsymbol{f}(\boldsymbol{x}) + \sum_{i=1}^{m} \boldsymbol{g}_i(\boldsymbol{x})\boldsymbol{u}_i, & i = 1, \ldots, m \\ y_j = h_j(\boldsymbol{x}), & j = 1, \ldots, m \end{cases} \tag{9}$$

where $\boldsymbol{x} \in \mathbb{R}^n$, $\boldsymbol{f}(\boldsymbol{x})$ and $\boldsymbol{g}_i(\boldsymbol{x})$ are the nonlinear smooth vector fields on $\boldsymbol{f} \in \mathbb{R}^n$ and $\boldsymbol{g}_i \in \mathbb{R}^n$, $h_j(\boldsymbol{x})$ are the nonlinear smooth scalar functions. The definitions of the kth Lie derivative of $h_j(\boldsymbol{x})$, $L_{g_i} L_f^k h_j(\boldsymbol{x})$, with respect to $\boldsymbol{f}(\boldsymbol{x})$ and $\boldsymbol{g}_i(\boldsymbol{x})$, are given by (10). And the relative order r_j for the jth output y_j is defined by (11)

$$\begin{aligned} &L_f^1 h_j(\boldsymbol{x}) = \frac{\partial h_j(\boldsymbol{x})}{\partial \boldsymbol{x}} f(\boldsymbol{x}), \quad L_f^k h_j(\boldsymbol{x}) = L_f(L_f^{k-1} h_j(\boldsymbol{x})) \\ &L_{g_i} L_f^k h_j(\boldsymbol{x}) = \frac{\partial L_f^k h_j(\boldsymbol{x})}{\partial \boldsymbol{x}} g_i(\boldsymbol{x}) \end{aligned} \tag{10}$$

$$\begin{cases} L_{g_i} L_f^k h_j(\boldsymbol{x}) = 0, \ k = 0, \ldots, \boldsymbol{r}_j - 2 \\ \exists l \in [1, \ldots, m], \quad L_{g_l} L_f^{\boldsymbol{r}_j - 1} h_j(\boldsymbol{x}) \neq 0 \end{cases}. \tag{11}$$

Then, the high-order derivatives of the system outputs y_j with the relative order r_j can be expressed as

$$\begin{cases} \dfrac{d^s y_j}{dt^s} = L_f^s h_j(\boldsymbol{x}), \quad s = 1, \ldots, r_j - 1 \\ \dfrac{d^{r_j} y_j}{dt^{r_j}} = L_f^{r_j} h_j(\boldsymbol{x}) + \sum_{i=1}^{m} L_{g_i} L_f^{r_j - 1} h_j(\boldsymbol{x}) \cdot \boldsymbol{u}_i. \end{cases} \tag{12}$$

To achieve a linear relationship between one input and the particular output y_j, the coordinate mapping associated with the new defined state variable $\epsilon_{j(p)}$ and the new defined input φ_j can be selected as

$$\begin{cases} \epsilon_{j(p)} = L_f^p h_j(\boldsymbol{x}), \quad p = 0, \ldots, r_j - 1 \\ \epsilon_{j(r_j)} = L_f^{r_j} h_j(\boldsymbol{x}) + \sum_{i=1}^{m} L_{g_i} L_f^{r_j - 1} h_j(\boldsymbol{x}) \cdot \boldsymbol{u}_i = \varphi_j. \end{cases} \tag{13}$$

Then, the original system shown in (9) will be transformed to an input–output linearized and decoupled system shown as

$$\begin{cases} \dot{\eta} = f_0(\eta, \epsilon_{j(p)} \cdots) \\ \dot{\epsilon}_{j(p)} = \epsilon_{j(p+1)}, \quad p = 0, \ldots, r_j - 2 \\ \dot{\epsilon}_{j(r_j - 1)} = \epsilon_{j(r_j)} = \varphi_j \\ y_j = \epsilon_{j(0)} \end{cases} \tag{14}$$

where $r_1 + \cdots + r_m = r_0, \boldsymbol{\eta} \in \mathbb{R}^{n - r_0}$. If $r_0 = n$, $\boldsymbol{\eta}$ will not exist and the original MIMO system is comprehensively linearized. Otherwise, the original system shown in (9) will be divided into two parallel subsystems: the system linearized dynamic and the system zero dynamic. And the $\boldsymbol{\eta}$ are the state variables of the system zero dynamics. Therefore, according to (13), the original system inputs u_j are exhibited as

$$\boldsymbol{u} = \boldsymbol{C}^{-1}(\boldsymbol{x})\left[\boldsymbol{\varphi} - \boldsymbol{\alpha}(\boldsymbol{x})\right] \tag{15}$$

where $\boldsymbol{u}^T = [u_1, \ldots, u_m]$, $\boldsymbol{\varphi}^T = [\varphi_1, \ldots, \varphi_m]$, $\boldsymbol{\alpha}(\boldsymbol{x})^T = [L_f^{r_1} h_j(\boldsymbol{x}), \ldots, L_f^{r_m} h_j(\boldsymbol{x})]$, and

$$\boldsymbol{C}(\boldsymbol{x}) = \begin{bmatrix} L_{g_1} L_f^{r_1 - 1} h_1(\boldsymbol{x}) & \cdots & L_{g_m} L_f^{r_1 - 1} h_1(\boldsymbol{x}) \\ \vdots & \ddots & \vdots \\ L_{g_1} L_f^{r_m - 1} h_m(\boldsymbol{x}) & \cdots & L_{g_m} L_f^{r_m - 1} h_m(\boldsymbol{x}) \end{bmatrix}. \tag{16}$$

Theorem 2 of Ref. [31] indicates that the following conditions are sufficient for the system shown in (9) to be input–output linearizable.

1) Each output y_j possesses a relative order r_j.
2) The matrix $\boldsymbol{C}(\boldsymbol{x})$ is nonsingular for all $\boldsymbol{x}$.

B. Phase-Unsynchronized Power Decoupling Control for MMC

The MMC plant given by (7) needs to be checked if it is input–output linearizable. Since $y_1 = h_1(x) = 1.5(v_d i_d + v_q i_q)$ and $y_2 = h_2(x) = 1.5(v_q i_d - v_d i_q)$, the relative orders of each output in (7) are calculated as

$$\begin{aligned}
L_{g_1}L_f^0 h_1(\boldsymbol{x}) &= 1.5c_6 v_d v^{\mathrm{dc}} + 0.75c_6\left(v_d v_d^{2\omega_0} + v_q v_q^{2\omega_0}\right)\\
L_{g_2}L_f^0 h_1(\boldsymbol{x}) &= 1.5c_6 v_q v^{\mathrm{dc}} + 0.75c_6\left(v_q v_d^{2\omega_0} + v_d v_q^{2\omega_0}\right)\\
L_{g_1}L_f^0 h_2(\boldsymbol{x}) &= 1.5c_6 v_q v^{\mathrm{dc}} + 0.75c_6\left(v_q v_d^{2\omega_0} - v_d v_q^{2\omega_0}\right)\\
L_{g_2}L_f^0 h_2(\boldsymbol{x}) &= -1.5c_6 v_d v^{\mathrm{dc}} + 0.75c_6\left(v_d v_d^{2\omega_0} + v_q v_q^{2\omega_0}\right)
\end{aligned} \tag{17}$$

and the relative orders of y_1 and y_2 are $r_1 = r_2 = 1$.

According to (16) and (17), the determinant of matrix $\boldsymbol{C}(\boldsymbol{x})$ is calculated and shown as follows:

$$\det\left[\boldsymbol{C}(\boldsymbol{x})\right] = \frac{9}{16}c_6^2(v_d^2 + v_q^2)\left[(v_d^{2\omega_0})^2 + (v_q^{2\omega_0})^2 - 4(v^{\mathrm{dc}})^2\right]. \tag{18}$$

In the normal operation, the magnitude of PCC voltage is nonzero, i.e., $v_d^2 + v_q^2 \neq 0$. Meanwhile, the value of v^{dc} is quite greater than that of $(v_d^{2\omega_0})^2 + (v_q^{2\omega_0})^2$. Thus, $\boldsymbol{C}(\boldsymbol{x})$ is nonsingular and based on Theorem 2 of [31], the MMC plant shown in (7) is input–output linearizable.

According to the dynamics of the fundamental-frequency currents shown in (A2), the MMC power dynamic is given as follows:

$$\begin{aligned}
\begin{bmatrix}\dot{P}\\ \dot{Q}\end{bmatrix} &= \frac{3}{2}\begin{bmatrix}v_d & v_q\\ v_q & -v_d\end{bmatrix}\begin{bmatrix}\dot{i_d}\\ \dot{i_q}\end{bmatrix} = \boldsymbol{M}_0\begin{bmatrix}\dot{i_d}\\ \dot{i_q}\end{bmatrix}\\
&= \boldsymbol{M}_0\left(-\begin{bmatrix}b_1\\ b_2\end{bmatrix} + \boldsymbol{M}_1\begin{bmatrix}v_d^{\mathrm{ref}}\\ v_q^{\mathrm{ref}}\end{bmatrix}\right) = \begin{bmatrix}\varphi_1^{\mathrm{ref}}\\ \varphi_2^{\mathrm{ref}}\end{bmatrix}
\end{aligned} \tag{19}$$

where

$$\begin{aligned}
b_1 &= c_4 i_d - \omega_0 i_q + 2c_5 v_d + c_5 v_d^{\omega_0}\\
b_2 &= c_4 i_q + \omega_0 i_d + 2c_5 v_q + c_5 v_q^{\omega_0}\\
\boldsymbol{M}_1 &= \begin{bmatrix}c_6 v^{\mathrm{dc}} + \frac{1}{2}c_6 v_d^{2\omega_0} & \frac{1}{2}c_6 v_q^{2\omega_0}\\ \frac{1}{2}c_6 v_q^{2\omega_0} & c_6 v^{\mathrm{dc}} - \frac{1}{2}c_6 v_d^{2\omega_0}\end{bmatrix}.
\end{aligned} \tag{20}$$

Following (19), the original input v_d^{ref} and v_q^{ref} are calculated as follows:

$$\begin{aligned}
\begin{bmatrix}v_d^{\mathrm{ref}}\\ v_q^{\mathrm{ref}}\end{bmatrix} &= \boldsymbol{M}_1^{-1}\left(\begin{bmatrix}b_1\\ b_2\end{bmatrix} + \boldsymbol{M}_0^{-1}\begin{bmatrix}\varphi_1^{\mathrm{ref}}\\ \varphi_2^{\mathrm{ref}}\end{bmatrix}\right)\\
&= \frac{1}{b_0}\begin{bmatrix}2v_d^{2\omega_0} - 4v^{\mathrm{dc}} & 2v_q^{2\omega_0}\\ 2v_q^{2\omega_0} & -2v_d^{2\omega_0} - 4v^{\mathrm{dc}}\end{bmatrix}\begin{bmatrix}b_1 + b_3\\ b_2 + b_4\end{bmatrix}
\end{aligned} \tag{21}$$

where

$$\begin{aligned}
b_0 &= c_6\left[(v_d^{2\omega_0})^2 + (v_q^{2\omega_0})^2 - 4(v^{\mathrm{dc}})^2\right]\\
b_3 &= \frac{2}{3(v_d^2 + v_q^2)}(v_d\varphi_1^{\mathrm{ref}} + v_q\varphi_2^{\mathrm{ref}})\\
b_4 &= \frac{2}{3(v_d^2 + v_q^2)}(v_q\varphi_1^{\mathrm{ref}} - v_d\varphi_2^{\mathrm{ref}}).
\end{aligned} \tag{22}$$

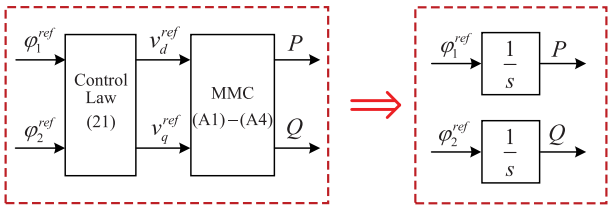

Fig. 2. Decoupling relationships between inputs φ_1^{ref}, φ_2^{ref} and outputs P, Q after input–output linearization.

Thus, the linearized relationships between the new inputs φ_1^{ref}, φ_2^{ref} and the active and reactive powers of MMC as system outputs are shown in Fig. 2. The power decoupling is achieved by the state feedback and the coordination transformation, which does not need phase information. Thus, the phase-synchronization is avoided, i.e., PLL is eliminated.

To ensure the reference tracking, integral elements are involved in the design of the secondary control loop for generating φ_1^{ref} and φ_2^{ref}. The MMC power dynamic response will be designed as the second-order system. Thus, using the active power P as an example to demonstrate the design of the secondary control loop, the integral element for the active power reference P_{ref} is given as follows:

$$\delta\dot{P} = P_{\mathrm{ref}} - P. \tag{23}$$

To simplify the control design, all loops are transformed to the s-domain. Equations (19) and (23) in the s-domain are expressed as follows:

$$sP(s) = \varphi_1^{\mathrm{ref}}(s), \quad s\delta P(s) = P_{\mathrm{ref}}(s) - P(s). \tag{24}$$

$\varphi_1^{\mathrm{ref}}(s)$ can be determined by P, P_{ref}, and δP as

$$\varphi_1^{\mathrm{ref}}(s) = G_1(s)\delta P(s) + G_2(s)P(s) + G_3(s)P_{\mathrm{ref}}(s). \tag{25}$$

Then, combining (24) and (25), P can be expressed as

$$P(s) = \frac{G_1(s) + sG_3(s)}{s^2 - sG_2(s) + G_1(s)}P_{\mathrm{ref}}(s). \tag{26}$$

To achieve the desired dynamics, $G_1(s)$, $G_2(s)$, and $G_3(s)$ can be determined by

$$G_1(s) = \omega_P^2, \quad G_2(s) = -2\xi_P\omega_P, \quad G_3(s) = 0. \tag{27}$$

Therefore, the state-space functions of the secondary control loops are shown in (28) and the whole linearized system is the minimum-phase realization.

$$\begin{aligned}
\varphi_1^{ref} &= \omega_P^2\delta P - 2\xi_P\omega_P P, \quad \delta\dot{P} = P_{\mathrm{ref}} - P\\
\varphi_2^{ref} &= \omega_Q^2\delta Q - 2\xi_Q\omega_Q Q, \quad \delta\dot{Q} = Q_{\mathrm{ref}} - Q.
\end{aligned} \tag{28}$$

As aforementioned, the control parameters of the inner loop comes from the system parameters. Considering parameter variations, they can be corrected by measurements and try-and-error around their nominal values. The control parameters of the outer loop are ξ_P, ξ_Q, ω_P, and ω_Q. They can be determined by the user with desired power dynamics, e.g., overshoot and setting time. The dynamic responses of MMC output power, with the

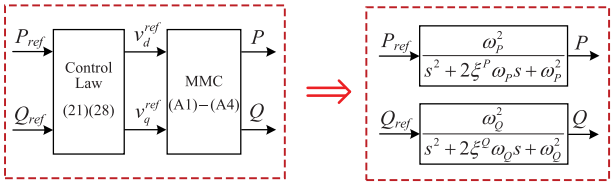

Fig. 3. Decoupling relationships between inputs P_{ref}, Q_{ref}, and outputs P, Q with designed second-order dynamics.

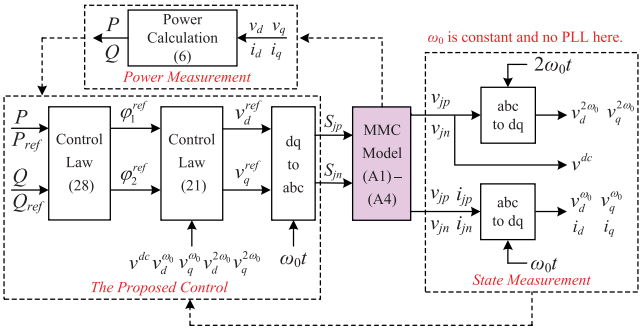

Fig. 4. Block diagram of the proposed control.

power reference P_{ref} and Q_{ref}, are shown in Fig. 3. The block diagram of the proposed control is shown in Fig. 4.

The desired state-space model of MMC with the proposed control is shown as follows:

$$\begin{cases} \dot{\boldsymbol{\eta}} = f_0'(\boldsymbol{\eta}, \boldsymbol{w}, \boldsymbol{u}, \xi_P, \xi_Q, \omega_P, \omega_Q, v_d, v_q, v_{\text{dc}}) \\ \dot{\boldsymbol{w}} = \boldsymbol{A}_1 \boldsymbol{w} + \boldsymbol{B}_1 \boldsymbol{u} \\ \boldsymbol{y} = \begin{bmatrix} 1\,0\,0\,0 \\ 0\,1\,0\,0 \end{bmatrix} \boldsymbol{w} \end{cases} \tag{29}$$

where $\boldsymbol{\eta}$ is the state variable vector of the system zero dynamic and $\boldsymbol{\eta}^T = [i_{\text{dc}}, v^{\text{dc}}, v_d^{\omega_0}, v_q^{\omega_0}, i_d^{2\omega_0}, i_q^{2\omega_0}, v_d^{2\omega_0}, v_q^{2\omega_0}]$, $\boldsymbol{w}$ is the state variable vector of the system linearized dynamic and $\boldsymbol{w}^T = [P, Q, \delta P, \delta Q]$, $\boldsymbol{u}$ is the MMC input vector and $\boldsymbol{u}^T = [P_{\text{ref}}, Q_{\text{ref}}]$. The matrices $\boldsymbol{A}_1$ and $\boldsymbol{B}_1$ are given as

$$A_1 = \begin{bmatrix} -2\xi_P\omega_P & 0 & \omega_P^2 & 0 \\ 0 & -2\xi_Q\omega_Q & 0 & \omega_Q^2 \\ -1 & 0 & 0 & 0 \\ 0 & -1 & 0 & 0 \end{bmatrix}, \quad B_1 = \begin{bmatrix} 0\,0 \\ 0\,0 \\ 1\,0 \\ 0\,1 \end{bmatrix}. \tag{30}$$

IV. Study Cases

A. Study System

A ±500-kV two-terminal MMC-HVdc study system is presented in Fig. 5 and the T equivalent circuit is adopted as the model of the 500-km dc transmission line. R_T, L_T, and C_T are the equivalent resistance, inductance, and capacitance of T circuit, respectively. L_s and C_g are the smoothing inductor and the grounding capacitor of dc system, respectively. The parameters of two MMCs in this study system are identical and MMC 2 will maintain the dc voltage of the study system. The parameters of the study system are given in Table I.

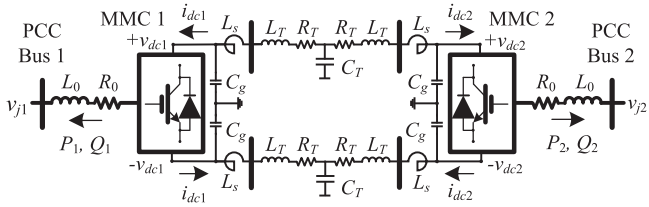

Fig. 5. Two-terminal MMC-HVdc study system.

TABLE I
Electric Parameters of Study System

Variables	Unit	Value	Variables	Unit	Value
C_{SM}	mF	20	R_T	Ω	6.365
L_{arm}	mH	0.1	L_T	mH	466.85
R_{arm}	Ω	3	C_T	μF	6.37
N		393	R_0	Ω	1
$\tilde{V}_{dc}$	kV	500	L_0	mH	0.2
L_s	mH	0.1	C_g	μF	1

B. Model Verification

To verify the developed MMC model with the proposed control, a comparison is conducted between the developed nonlinear state space model calculated in MATLAB and the circuit model simulated in PSCAD/EMTDC.

A step change on the active power reference P_{ref} of MMC 1 occurs from 70 to 220 MW at $t = 9$ s, meanwhile Q_{ref} keeps 100 Mvar. The dynamic responses of 10 state variables of MMC 1 are shown in Figs. 6 and 7, respectively. The calculation in MATLAB and the simulation in PSCAD/EMTDC present the highly identical behavior. The value deviations between simulations and calculations are extremely small, which can be neglected. Thus, the feasibility of the developed MMC model shown in (29) with the proposed control is validated.

C. Dynamics Comparison of Different Controls

First, two study cases are applied to demonstrate the dynamic transient and decoupling performance of the proposed control. To guarantee fair comparisons, the control parameters of the conventional dq controller and the proposed controller are determined to ensure the similar settling time. And the parameters of active power loop and reactive power loop are identical. In *case*-1, the active power reference P_{ref} of MMC 1 has a step change from 70 to 220 MW; meanwhile, the reactive power reference Q_{ref} maintains 100 MVar. In *case*-2, Q_{ref} of MMC 1 has a step change from 100 to 270 MVar; meanwhile, P_{ref} maintains 70 MW. The active power, reactive power, i_d, and i_q of two cases are shown in Figs. 8 and 9, respectively. In these two study cases, ξ_P, ξ_Q are 0.707 and ω_P, ω_Q regulate the associated control speed.

According to Figs. 8(a) and (b) and 9(a) and (b), the dynamic transients of the proposed control are the behaviors of typical second-order systems, as the desired design. Furthermore, considering the different power coupling principle of two-level VSC and MMC, the proposed control realizes the precise power decoupling performance of MMC power control.

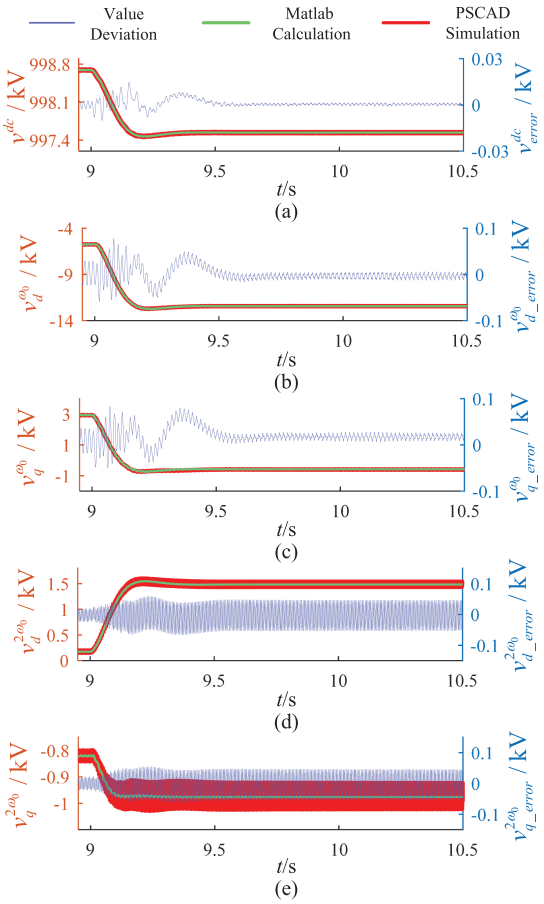

Fig. 6. Voltage dynamic responses of the MMC 1 and numerical comparisons between PSCAD/EMTDC simulation and MATLAB solution. (a) v^{dc}. (b) $v_d^{\omega_0}$. (c) $v_q^{\omega_0}$. (d) $v_d^{2\omega_0}$. (e) $v_q^{2\omega_0}$.

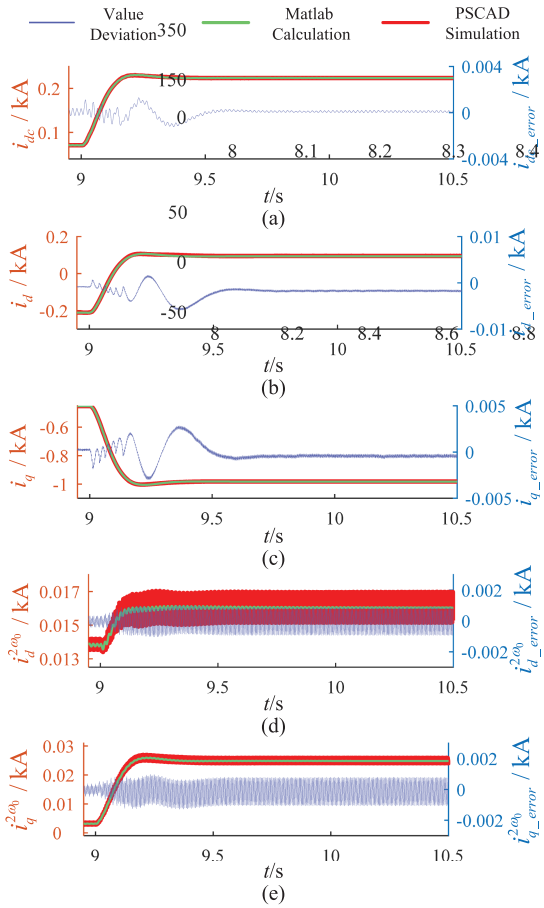

Fig. 7. Current dynamic responses of the MMC 1 and numerical comparisons between PSCAD/EMTDC simulation and MATLAB solution. (a) i_{dc}. (b) i_d. (c) i_q. (d) $i_d^{2\omega_0}$. (e) $i_q^{2\omega_0}$.

As the comparison, the conventional dq control is designed for two-level VSC without considering the MMC inner dynamics. It cannot eliminate the MMC power coupling and may bring worse performance with improper control parameters.

Additionally, Figs. 8(c) and (d) and 9(c) and (d) illustrate the dynamics of i_d and i_q, including transients and steady-state information. Table II provides the details of the power calculation at steady-state conditions containing v_d and v_q. According to Figs. 8(c) and (d) and 9(c) and (d), and Table II, it is validated that the power decoupling principle of the dq control depends on the phase synchronization achieved by PLL while that of the proposed control is realized by phase-unsynchronized state feedback and coordination transform. On the other side, the current transient dynamics of MMC with the conventional dq control shown in Figs. 8(c) and (d) and 9(c) and (d) also demonstrate that the conventional dq controller does not consider the influence of the MMC capacitor voltage dynamics, which deteriorates the performance of power decoupling.

Considering that the system parameters can be deviated from their nominal values, the simulations are performed to analyze the impact of the system parameter variations on the control performance. In the proposed method, the inner loop employs the arm inductance, arm resistance, PCC inductance, and PCC resistance to linearize the MMC model. Hence, four cases are shown in Table III. The associated simulation results are shown in Figs. 10 and 11, respectively. In Fig. 10, P_{ref} has a step change from 300 to 450 MW. In Fig. 11, Q_{ref} has a step change from 200 to 100 MVar. The gray lines in Figs. 10 and 11 are the dynamic reference that the control parameters are identical to the circuit parameters.The simulation results show that, although the arm inductance and the PCC inductance have the negative effect on the MMC power decoupling performance, the proposed control is still available for power control. Meanwhile, the arm resistance and PCC resistance have no evident effect on the proposed control. Therefore, the MMC inductance must be measured accurately to guarantee the performance of the proposed control.

On the other side, the drift of the grid frequency should also be investigated since the dq transformation in the proposed method maintains the nominal value. Fig. 12 shows the simulation results of *case*-7. In this case, the grid frequency has a step change from 60 to 58 Hz. The P_{ref} and Q_{ref} are 500 MW and -500 MVar, respectively. According to Fig. 12(a), there are transients during the grid frequency deviation due to that the impedances of the PPC inductance and the arm inductance have the corresponding step changing in the circuit. Thus, the compensation from the inner loop is enough so the integrators in the outer loop contributes

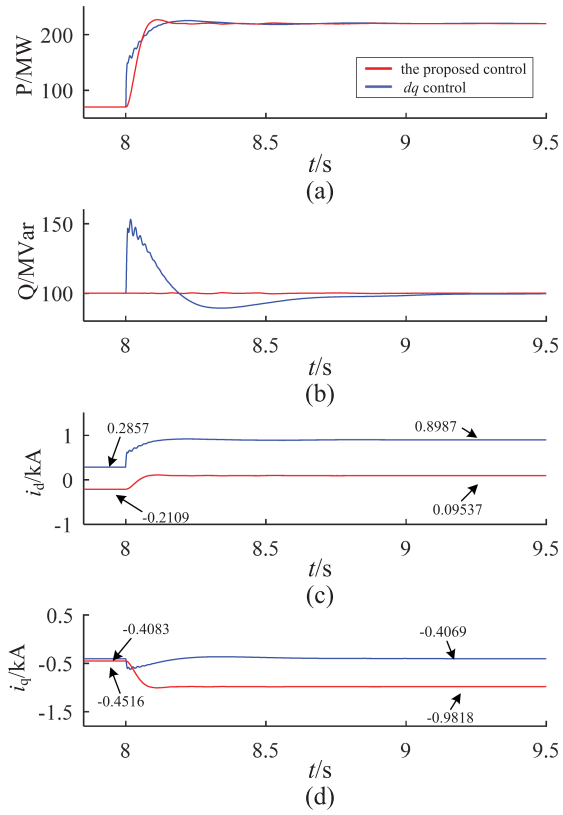

Fig. 8. Dynamic responses of power and current of MMC 1 in *case*-1. (a) P. (b) Q. (c) i_d. (d) i_q.

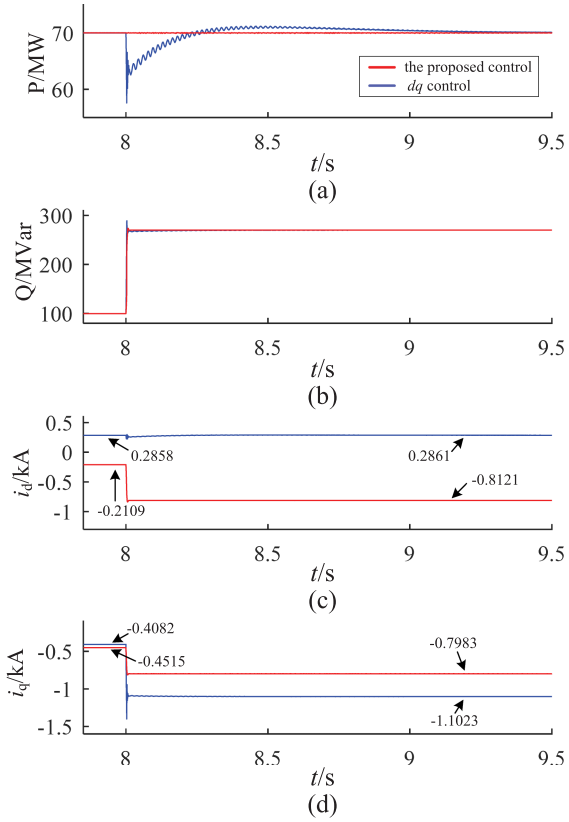

Fig. 9. Dynamic responses of power and current of MMC 1 in *case*-2. (a) P. (b) Q. (c) i_d. (d) i_q.

to the compensation for the grid frequency drift. In Fig. 12(b) and (c), v_d, v_q, i_d, and i_q become sinusoidal components instead of dc components. However, the MMC power can be controlled to its references since the state feedback is not affected by the numerical form of feedback state variables. As the conclusion, the grid frequency drift has no influence on the controllability of the proposed method but it can negatively affect on power decoupling as the system parameter variations of inductances.

D. Experimental Results

An experimental prototype of the three-phase grid-tied MMC is established to verify the validation of the proposed control method, as shown in Fig. 13. The schematic of this prototype is shown in Fig. 14. Moreover, the parameters of the prototype is illustrated in Table IV. In this prototype, the power analyzer measures the MMC-controlled active and reactive power. The ac power source and resister load are combined together to emulate the ac grid with four-quadrant power flow.

Considering the SM capacitor voltage unbalancing, the single-step alternated modulation method [32] is adopted to PWM implemented by FPGA instead of the conventional closed-loop individual capacitor voltage control, overall capacitor voltage control, and arm capacitor voltage control. The SM capacitor charging/discharging principle and the associated analysis of the alternated modulation method can be found in [33]. Since the MMC power control just generates reference for modulation

TABLE II
POWER CALCULATION OF THE *DQ* AND THE PROPOSED CONTROL

Step Change	v_d	v_q	i_d	i_q	P	Q
The *dq* Control in *case*-1						
Before	163.2993	0	0.2857	-0.4083	69.9819	100.0127
After	163.2993	0	0.8987	-0.4069	220.1356	99.6697
The Proposed Control in *case*-1						
Before	81.5963	-141.4521	-0.2109	-0.4516	70.0067	100.0217
After	81.5963	-141.4521	0.09537	-0.9818	219.9893	99.9315
The *dq* Control in *case*-2						
Before	163.2993	0	0.2858	-0.4082	70.0064	99.9882
After	163.2993	0	0.2861	-1.1023	70.0799	270.0073
The Proposed Control in *case*-2						
Before	81.5963	-141.4521	-0.2109	-0.4515	69.9855	100.0095
After	81.5963	-141.4521	-0.8121	-0.7983	69.9853	270.0174

TABLE III
CASES OF CIRCUIT PARAMETER VARIATION

Parameters	Circuit	Controller			
		case-3	*case*-4	*case*-5	*case*-6
Arm Inductance	0.1 H	0.12 H (+20%)	0.1 H	0.1 H	0.1 H
Arm Resistance	3 Ω	3 Ω	5 Ω (+66.7%)	3 Ω	3 Ω
PCC Inductance	0.2 H	0.2 H	0.2 H	0.15 H (-25%)	0.2 H
PCC Resistance	1 Ω	1 Ω	1 Ω	1 Ω	0.7 Ω (-30%)

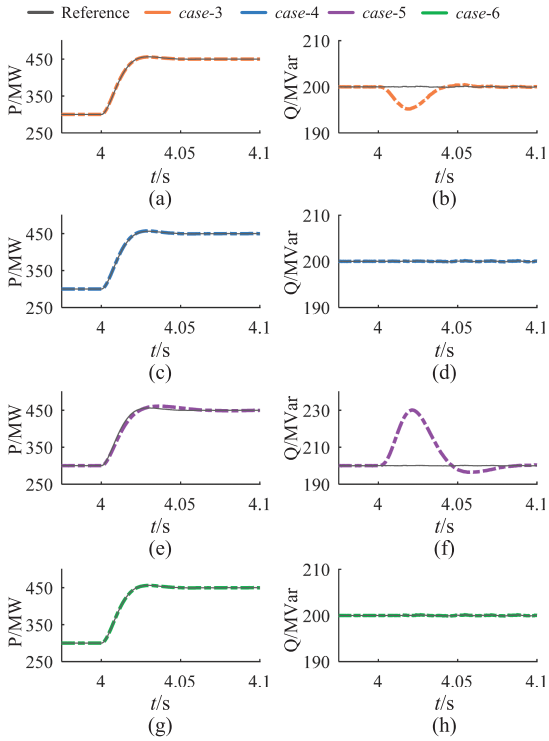

Fig. 10. Dynamic responses of active and reactive power of MMC 1 with system parameter variation when the active power reference has a step change from 300 to 450 MW. (a) and (b) Results of *case* 3. (c) and (d) Results of *case* 4. (e) and (f) Results of *case* 5. (g) and (h) Results of *case* 6.

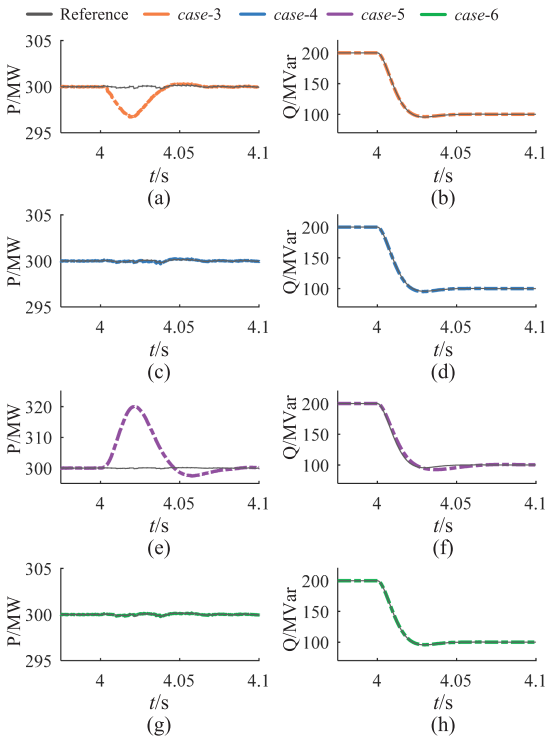

Fig. 11. Dynamic responses of active and reactive power of MMC 1 with system parameter variation when the reactive power reference has a step change from 200 MVar to 100 MVar. (a) and (b) are the results of *case* 3. (c) and (d) are the results of *case* 4. (e) and (f) are the results of *case* 5. And (g) and (h) are the results of *case* 6.

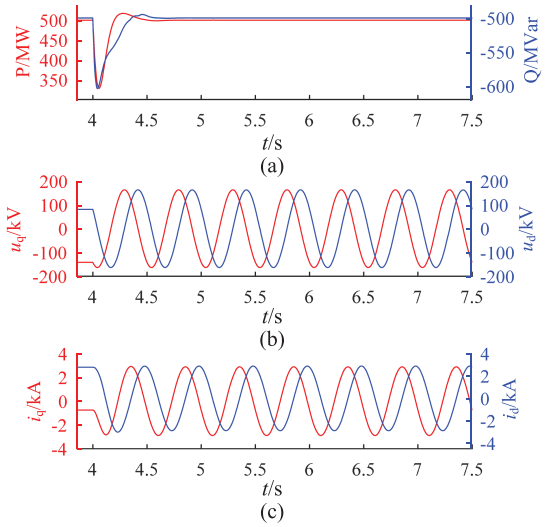

Fig. 12. Dynamic responses of active and reactive power of MMC 1 with grid frequency drift when the grid frequency has a step change from 60 to 58 Hz. (a) Dynamics of active and reactive power. (b) Dynamics of u_d and u_q of *case* 7. (c) Dynamics of i_d and i_q.

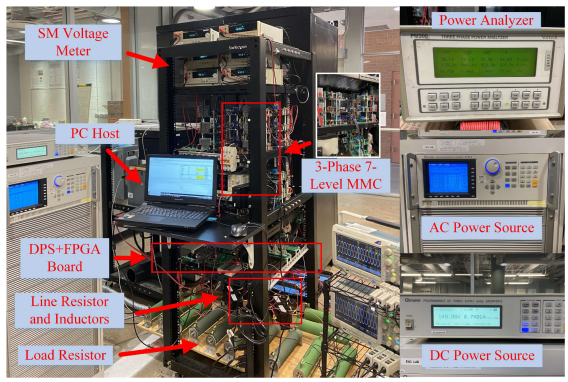

Fig. 13. Photograph of the experimental prototype.

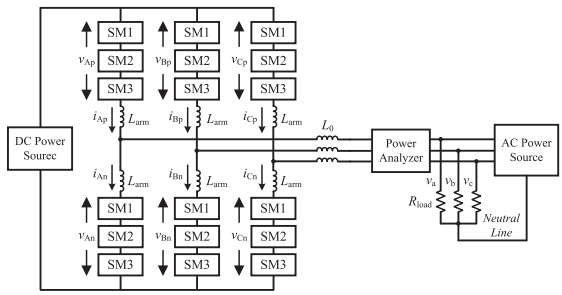

Fig. 14. Schematic of the experimental prototype.

in DSP, the modulation in FPGA will not have any negative effect on the MMC power control, i.e., dq control and the proposed control. The potential negative dynamic influence of the conventional closed-loop capacitor voltage control can be avoided.

Fig. 15 shows the MMC arm voltage, output voltage, and output currents as an operation test without ac power source

TABLE IV
ELECTRIC PARAMETERS OF EXPERIMENTAL PROTOTYPE

DC-link voltage, V_{dc}	150 V
SM capacitance, C_{SM}	1000 μF
Arm inductance, L_{arm}	4.1 mH
Number SM of per arm, N	3
AC-tied inductance, L_0	10 mH
Resistor load, R_{load}	4.167 Ω
AC side frequency, f_{ac}	50 Hz
AC-link L-G RMS voltage, $v_{a,b,c}$	35 V
Semiconductor device	FGH40T65UQDF

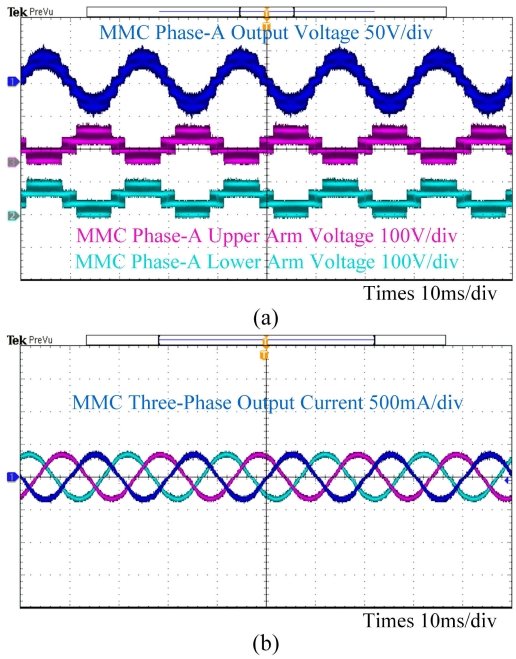

Fig. 15. Experimental results of MMC without grid connection when the dc-link voltage is 100 V and the resistor load is 100 Ω, respectively. (a) MMC phase a upper, lower, and output voltages. (b) MMC three-phase output currents.

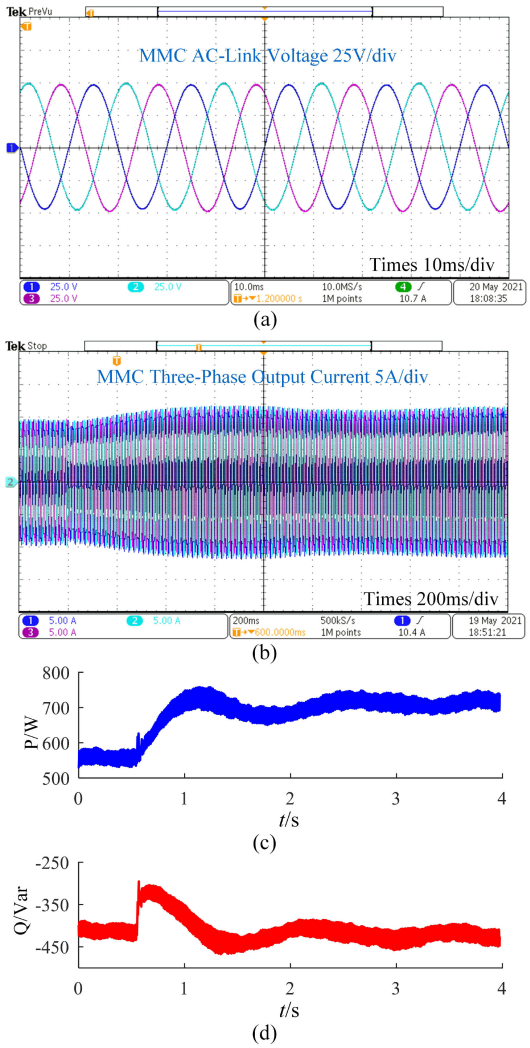

Fig. 16. Experimental results of MMC with the conventional dq controller when P_{ref} has a step change from 550 W to 700 W while Q_{ref} maintains minus;400 Var. (a) AC-link voltage. (b) MMC output current. (c) Active power dynamics. (d) Reactive power dynamics.

when the resistor load is 100 Ω. These results confirm that the prototype is working in good condition.

Then, Figs. 16 and 17 show the experimental results of the dq controller, including ac-link voltage, output current, and the power dynamics calculated by the records of two oscilloscopes. Since the ac-link voltages in different cases are identical, it is only displayed in Fig. 16. In Fig. 16, P_{ref} has a step change from 550 to 700 W; meanwhile, Q_{ref} keeps -400 Var. In Fig. 17, Q_{ref} has a step change from -400 Var to -550 Var meanwhile P_{ref} maintains 600 W. The measurements of the power analyzer at steady-state of these two cases are shown in Table V. According to the power dynamics shown in Figs. 16(c) and (d) and 17(b) and (c), the conventional dq control does not consider that each SM capacitor needs release/absorb energy, which further influences the arm voltage and inevitably brings out the power coupling. This phenomenon also supports the conclusion that the MMC inner dynamics have significant effect on the MMC power decoupling.

Figs. 18 and 19 show the experimental results of the proposed control while Table VI presents the measurements of power analyzer. As a comparison, the cases conditions for the proposed control verification are identical to the cases for dq controller. Compared with the power dynamics of dq controller shown in Figs. 16(c) and (d) and 17(b) and (c), the proposed controller compensates the MMC inner dynamics and achieves better performance on the power decoupling without PLL, as shown in Figs. 18(b) and (c) and 19(b) and (c). Since the frequency of ac power source must have a small drift from the settings while the circuit parameters must have deviations from their nominal values, the negative impact of them on the proposed control can be minimized through parameter measurements and adjustments. Thus, the effectiveness and benefits of the proposed control are verified through experimental results.

V. STABILITY ANALYSIS

In this section, the stability of the MMC with the proposed control will be analyzed. According to (29), the MMC stability is composed of the stability of the system zero dynamic $\boldsymbol{\eta}$ and that of the system linearized dynamic $\boldsymbol{w}$. The stability of the system-linearized dynamic is easy to be guaranteed by adjusting

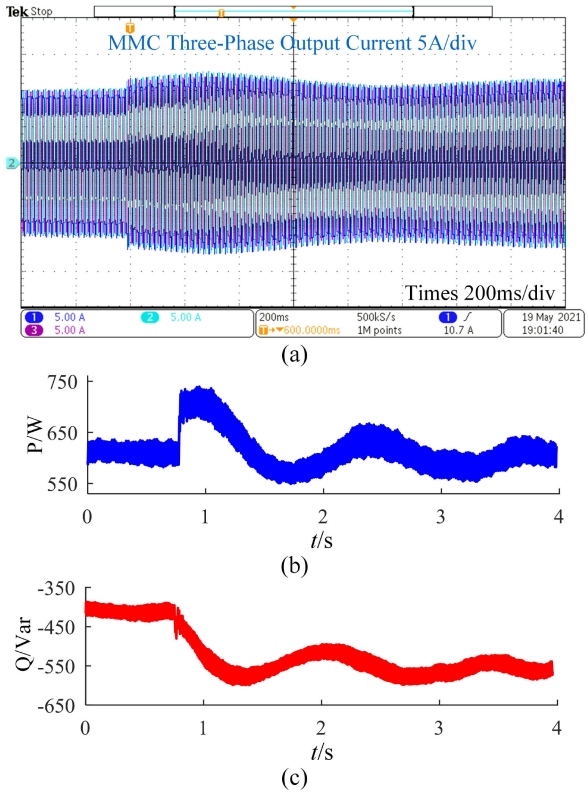

Fig. 17. Experimental results of MMC with the conventional dq controller when Q_{ref} has a step change from -400 Var to -550 Var while P_{ref} maintains 600 W. (a) MMC output current. (b) Active power dynamics. (c) Reactive power dynamics.

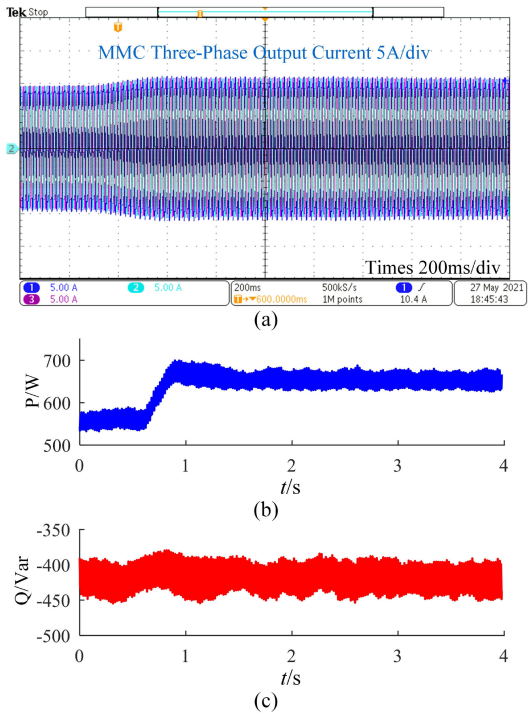

Fig. 18. Experimental results of MMC with the proposed controller when P_{ref} has a step change from 550 to 700 W while Q_{ref} maintains -400 Var. (a) MMC output current. (b) Active power dynamics. (c) Reactive power dynamics.

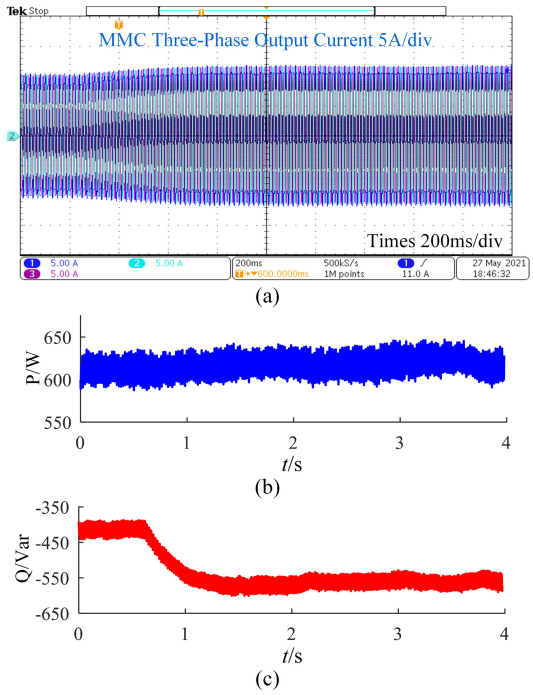

Fig. 19. Experimental results of MMC with the proposed controller when Q_{ref} has a step change from -400 to -550 Var while P_{ref} maintains 600 W. (a) MMC output current. (b) Active power dynamics. (c) Reactive power dynamics.

TABLE V
MEASUREMENTS OF THE POWER ANALYZER FOR THE dq CONTROL

Measurement	P_{ref} step changing		Q_{ref} step changing	
	Before	After	Before	After
v_a	35.01 V	35.17 V	35.06 V	35.03 V
v_b	35.09 V	35.21 V	35.14 V	35.13 V
v_c	34.75 V	34.86 V	34.79 V	34.75 V
i_a	6.813 A	8.163 A	7.269 A	8.225 A
i_b	6.886 A	8.280 A	7.361 A	8.352 A
i_c	6.592 A	7.897 A	7.030 A	7.987 A
P	574.1 W	740.6 W	629.8 W	632.2 W
Q	-416.2 Var	-424.4 Var	-419.6 Var	-582.9 Var

TABLE VI
MEASUREMENTS OF THE POWER ANALYZER FOR THE PROPOSED CONTROL

Measurement	P_{ref} step changing		Q_{ref} step changing	
	Before	After	Before	After
v_a	35.06 V	35.19 V	35.13 V	35.17 V
v_b	35.09 V	35.15 V	35.13 V	35.11 V
v_c	34.73 V	34.80 V	34.77 V	34.76 V
i_a	6.864 A	7.683 A	7.304 A	8.252 A
i_b	6.771 A	7.535 A	7.207 A	8.137 A
i_c	6.652 A	7.447 A	7.074 A	8.066 A
P	574.7 W	673.8 W	629.1 W	634.6 W
Q	-414.5 Var	-421.1 Var	-417.9 Var	-574.2 Var

the parameters ξ_P, ξ_Q, ω_P, and ω_Q. Hence, the MMC stability will only depend on the stability of the system zero dynamic. Due to its nonlinearity, the first theorem of Lyapunov stability theory is applied to analyze the stability of the system zero dynamic which is affected by the power system parameters v_d, v_q, v_{dc}, the equilibrium point P_{ref}, Q_{ref}, and the control parameters ξ_P, ξ_Q, ω_P, ω_Q.

TABLE VII
EIGENVALUE DISTRIBUTION OF DIFFERENT PARAMETER VARIATIONS

Varied Parameter	Varying Range	Varying Step	Max Deviation ($\times 10^{-12}$)	Min Deviation ($\times 10^{-12}$)
Equilibrium 1, $P = 1500MW$, $Q = 100MVar$				
v_d, v_q	$\angle\theta : 0 \sim 2\pi$	0.1	3.9464	0.9603
ξ_P	$0.1 \sim 5$	0.01	4.6216	1.8565
ξ_Q	$0.1 \sim 5$	0.01	4.3781	1.4648
ω_P	$1 \sim 800$	1	4.1402	1.2397
ω_Q	$1 \sim 800$	1	4.3651	1.1175
Equilibrium 2, $P = -500MW$, $Q = 1100MVar$				
v_d, v_q	$\angle\theta : 0 \sim 2\pi$	0.1	3.8199	1.0320
ξ_P	$0.1 \sim 5$	0.01	5.2287	1.6314
ξ_Q	$0.1 \sim 5$	0.01	4.6550	1.8466
ω_P	$1 \sim 800$	1	4.0323	1.6769
ω_Q	$1 \sim 800$	1	4.3583	1.3066

At first, the system zero dynamic stability is investigated along with the varying control parameters ξ_P, ξ_Q, ω_P, and ω_Q. Considering the impact of different equilibrium points, two operating points $P = 1500$ MW, $Q = 100$ MVar, and $P = -500$ MW, $Q = 1100$ MVar are selected. Along with these four parameters varying, all eigenvalues maintain constant. The details are shown in Table VII. The maximum and minimum deviations shown in Table VII are the maximum and minimum deviated distances among all eigenvalues calculated with varied parameters, respectively. Therefore, it is concluded that ξ_P, ξ_Q, ω_P, and ω_Q have no influence on the system zero dynamic stability under different equilibrium points.

Then, the system zero dynamic stability is studied along with the varying power system parameters v_d, v_q, and v_{dc}. To obtain different values of v_d and v_q, there are two methods: different initial phase angle $\angle\theta$ with constant phase voltage magnitude $|v|$, and constant $\angle\theta$ with different $|v|$. In the first situation, $|v|$ is 163.2993 kV and, along with the varying $\angle\theta$, the eigenvalues of the system zero dynamic maintain constant. The details are shown in Table VII as well. This phenomenon expresses that the initial phase angle of the ac voltage of PCC bus does not affect the MMC stability. In the second situation, the phase voltage magnitude $|v|$ varies from 100 to 200 kV and the initial phase angle is $-\pi/3$. At two equilibrium points, the associated eigenvalue loci are displayed in Fig. 20, which demonstrates that the magnitude of ac phase voltage has impacts on the system zero dynamic stability but the impacts are limited. Considering the normal operating conditions, the voltage variation of PCC bus has a negligible effect on the MMC stability.

In addition, the variation of the dc voltage may affect the system zero dynamic stability. When v_{dc} varies from 450 to 550 kV, the corresponding eigenvalue locus is presented in Fig. 21, which shows that the influence of the MMC dc-side voltage can be neglected.

Finally, the influence of different equilibrium points on the system zero dynamic stability is analyzed. The capacities of two MMC in the study system are 1500 MVA. The stable operation regions are obtained through checking the eigenvalues of the system zero dynamic. The intercepts of horizontal and vertical axises are 1 MW and 1 MVar, respectively. To further validate that the influences caused by the power system parameters are

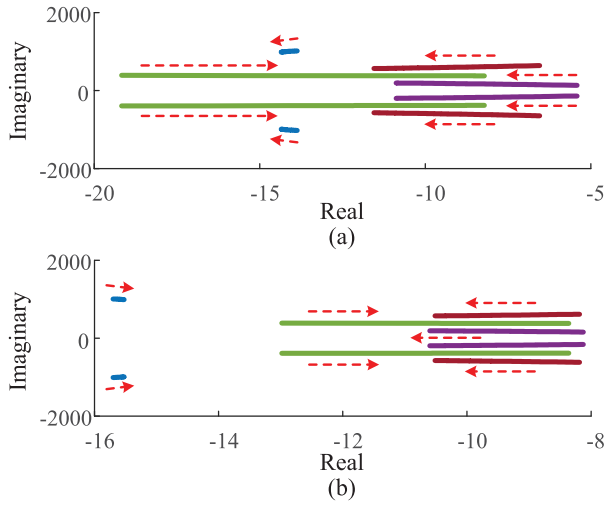

Fig. 20. Eigenvalue loci of the system zero dynamic associated with the varying magnitude of ac voltage. (a) *Equilibrium*-1. (b) *Equilibrium*-2.

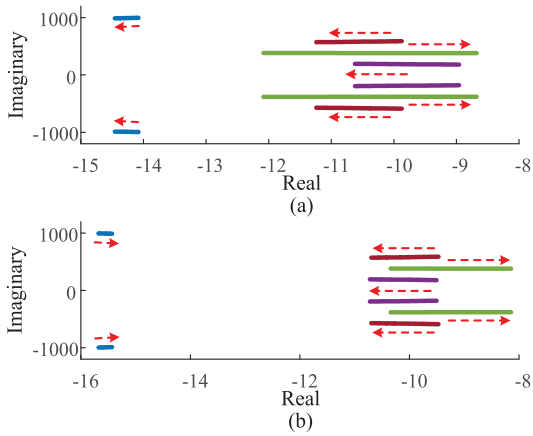

Fig. 21. Eigenvalue loci of the system zero dynamic associated with the varying MMC dc-side voltage. (a) *Equilibrium*-1. (b) *Equilibrium*-2.

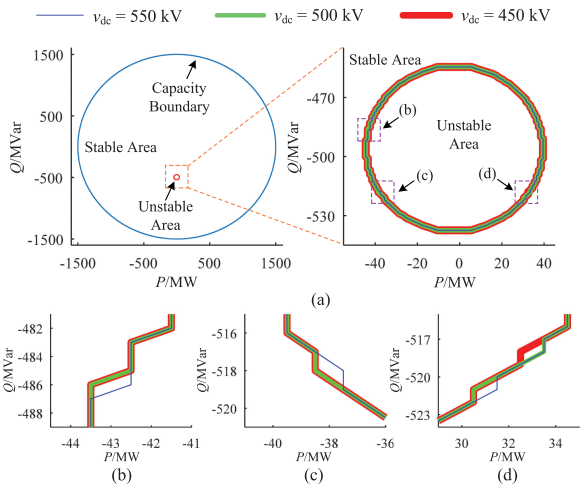

Fig. 22. Stability map of the system zero dynamic with different operation points and MMC dc-side voltage. (a) Overall stability map and local magnification of the unstable area. (b)–(d) Further local magnification for the boundary comparison of different unstable areas.

negligible, different dc voltages are adopted. The results are exhibited in Fig. 22. There is a very small region in each case causing the MMC inner dynamic unstable, even though the MMC input–output dynamic maintains stable. This unstable area is generated by the control structure shown in (21). Thus, the application of the proposed control needs to consider the region of operating point.

Moreover, compared with the boundaries of the unstable operation regions with different $v_{\rm dc}$, there are only four minuscule differences. Each difference means one equilibrium point with the associated intercepts. Thus, Fig. 22 supports the conclusion that the effect on the system stability caused by the MMC dc-side voltage can be ignored under normal operation.

VI. Conclusion

This article presents a phase-unsynchronized power decoupling control for MMC without PLL, and further analyzes the stability of MMC with the proposed control through the eigenvalue evaluation of the system zero dynamic. The power dynamics of MMC are designed as the second-order system so that the control parameters can be easily determined to satisfy the required transient specifications. Compared with the conventional *dq* controller, the simulations in PSCAD/EMTDC and the experimental results demonstrate the advantages of the proposed control, i.e., compensating MMC inner dynamics, eliminating PLL, guaranteeing power decoupling, and achieving better power dynamics. After investigating the influences of the control parameters, power system parameters, and the operating points, the stability analysis shows that the stability of the MMC with the proposed method can be guaranteed under the normal operation condition covering the most operating region of the MMC capacity limitation.

Appendix

The dynamics of the dc voltage and current of arms are as follows:

$$\begin{aligned}\dot{i}_{\rm dc} &= -c_1 i_{\rm dc} + c_2 v_{\rm dc} - \frac{1}{2}c_2 v^{\rm dc} + 3c_3\left(v_d^{\omega_0} v_d^{\rm ref} + v_q^{\omega_0} v_q^{\rm ref}\right)\\ \dot{v}_{\rm dc} &= \frac{2}{3}c_7 i_{\rm dc} - c_8\left(i_d v_d^{\rm ref} + i_q v_q^{\rm ref}\right).\end{aligned} \tag{A1}$$

The dynamics of the fundamental frequency voltage and current of arms are as follows:

$$\begin{aligned}\dot{v}_d^{\omega_0} &= c_7 i_d + \omega_0 v_q^{\omega_0} - \frac{2}{3}c_8 i_{\rm dc} v_d^{\rm ref} - 2c_8\left(i_d^{2\omega_0} v_d^{\rm ref} + i_q^{2\omega_0} v_q^{\rm ref}\right)\\ \dot{v}_q^{\omega_0} &= c_7 i_q - \omega_0 v_d^{\omega_0} - \frac{2}{3}c_8 i_{\rm dc} v_q^{\rm ref} - 2c_8\left(i_q^{2\omega_0} v_d^{\rm ref} - i_d^{2\omega_0} v_q^{\rm ref}\right)\\ \dot{i}_d &= -c_4 i_d + \omega_0 i_q - 2c_5 v_d - c_5 v_d^{\omega_0} + c_6 v^{\rm dc} v_d^{\rm ref}\\ &\quad + \frac{1}{2}c_6\left(v_d^{\rm ref} v_d^{2\omega_0} + v_q^{\rm ref} v_q^{2\omega_0}\right)\\ \dot{i}_q &= -c_4 i_q - \omega_0 i_d - 2c_5 v_q - c_5 v_q^{\omega_0} + c_6 v^{\rm dc} v_q^{\rm ref}\\ &\quad + \frac{1}{2}c_6\left(v_d^{\rm ref} v_q^{2\omega_0} - v_q^{\rm ref} v_d^{2\omega_0}\right).\end{aligned} \tag{A2}$$

The dynamics of the second-order harmonic voltage and current of arms are as follows:

$$\begin{aligned}\dot{v}_d^{2\omega_0} &= 2c_7 i_d^{2\omega_0} + 2\omega_0 v_q^{2\omega_0} - c_8\left(i_d v_d^{\rm ref} - i_q v_q^{\rm ref}\right)\\ \dot{v}_q^{2\omega_0} &= 2c_7 i_q^{2\omega_0} - 2\omega_0 v_d^{2\omega_0} - c_8\left(i_q v_d^{\rm ref} + i_d v_q^{\rm ref}\right)\\ \dot{i}_d^{2\omega_0} &= -c_1 i_d^{2\omega_0} + 2\omega_0 i_q^{2\omega_0} + c_3\left(v_d^{\omega_0} v_d^{\rm ref} - v_q^{\omega_0} v_q^{\rm ref}\right)\\ \dot{i}_q^{2\omega_0} &= -c_1 i_q^{2\omega_0} - 2\omega_0 i_d^{2\omega_0} + c_3\left(v_d^{\omega_0} v_q^{\rm ref} + v_q^{\omega_0} v_d^{\rm ref}\right).\end{aligned} \tag{A3}$$

The coefficients of (A1), (A2), and (A3) are as follows:

$$\begin{aligned}&c_1 = \frac{R_{\rm arm}}{L_{\rm arm}}, c_2 = \frac{3}{L_{\rm arm}}, c_3 = \frac{c_2}{12\tilde{V}_{\rm dc}}, c_4 = \frac{2R_0 + R_{\rm arm}}{2L_0 + L_{\rm arm}}\\ &c_5 = \frac{1}{2L_0 + L_{\rm arm}}, c_6 = \frac{c_5}{\tilde{V}_{\rm dc}}, c_7 = \frac{N}{4C_{SM}}, c_8 = \frac{3c_7}{4\tilde{V}_{\rm dc}}.\end{aligned} \tag{A4}$$

References

[1] L. Zhang *et al.*, "Modeling, control, and protection of modular multilevel converter-based multi-terminal HVDC systems: A review," *CSEE J. Power Energy Syst.*, vol. 3, no. 4, pp. 340–352, 2017.

[2] A. Dekka, B. Wu, R. L. Fuentes, M. Perez, and N. R. Zargari, "Evolution of topologies, modeling, control schemes, and applications of modular multilevel converters," *IEEE Trans. Emerg. Sel. Topics Power Electron.*, vol. 5, no. 4, pp. 1631–1656, Dec. 2017.

[3] Q. Hao, Z. Li, F. Gao, and J. Zhang, "Reduced-order small-signal models of modular multilevel converter and MMC-based HVdc grid," *IEEE Trans. Ind. Electron.*, vol. 66, no. 3, pp. 2257–2268, Mar. 2019.

[4] F. Blaabjerg, R. Teodorescu, M. Liserre, and A. V. Timbus, "Overview of control and grid synchronization for distributed power generation systems," *IEEE Trans. Ind. Electron.*, vol. 53, no. 5, pp. 1398–1409, Oct. 2006.

[5] S.-Y. Ruan, G.-J. Li, L. Peng, Y.-Z. Sun, and T. Lie, "A nonlinear control for enhancing HVDC light transmission system stability," *Int. J. Elect. Power Energy Syst.*, vol. 29, no. 7, pp. 565–570, 2007.

[6] M. Saeedifard and R. Iravani, "Dynamic performance of a modular multilevel back-to-back HVdc system," *IEEE Trans. Power Del.*, vol. 25, no. 4, pp. 2903–2912, Oct. 2010.

[7] R. Lizana, M. A. Perez, D. Arancibia, J. R. Espinoza, and J. Rodriguez, "Decoupled current model and control of modular multilevel converters," *IEEE Trans. Ind. Electron.*, vol. 62, no. 9, pp. 5382–5392, Sep. 2015.

[8] J. Z. Zhou, H. Ding, S. Fan, Y. Zhang, and A. M. Gole, "Impact of short-circuit ratio and phase-locked-loop parameters on the small-signal behavior of a VSC-HVdc converter," *IEEE Trans. Power Del.*, vol. 29, no. 5, pp. 2287–2296, Oct. 2014.

[9] M. F. M. Arani and Y. A. -R. I. Mohamed, "Analysis and performance enhancement of vector-controlled VSC in HVdc links connected to very weak grids," *IEEE Trans. Power Syst.*, vol. 32, no. 1, pp. 684–693, Jan. 2017.

[10] D. Dong, B. Wen, D. Boroyevich, P. Mattavelli, and Y. Xue, "Analysis of phase-locked loop low-frequency stability in three-phase grid-connected power converters considering impedance interactions," *IEEE Trans. Ind. Electron.*, vol. 62, no. 1, pp. 310–321, Jan. 2015.

[11] S. Sang, N. Gao, X. Cai, and R. Li, "A novel power-voltage control strategy for the grid-tied inverter to raise the rated power injection level in a weak grid," *IEEE Trans. Emerg. Sel. Topics Power Electron.*, vol. 6, no. 1, pp. 219–232, Mar. 2018.

[12] J. Wang and P. Wang, "Power decoupling control for modular multilevel converter," *IEEE Trans. Power Electron.*, vol. 33, no. 11, pp. 9296–9309, Nov. 2018.

[13] J. Wang, P. Wang, M. Zagrodnik, S. Mukherjee, and D. Vaidya, "A modulation reference compensation method to realize fully decoupled power control for modular multilevel converters," *IEEE Trans. Power Electron.*, vol. 34, no. 8, pp. 7230–7241, Aug. 2019.

[14] J. Wang and P. Wang, "Decoupled power control for direct-modulation-based modular multilevel converter with improved stability," *IEEE Trans. Ind. Electron.*, vol. 66, no. 7, pp. 5264–5274, Jul. 2019.

[15] H. K. Khalil and J. W. Grizzle, *Nonlinear Systems*, vol. 3. Upper Saddle River, NJ, USA: Prentice Hall, 2002.

[16] C. Xia, Q. Geng, X. Gu, T. Shi, and Z. Song, "Input–output feedback linearization and speed control of a surface permanent-magnet synchronous wind generator with the boost-chopper converter," *IEEE Trans. Ind. Electron.*, vol. 59, no. 9, pp. 3489–3500, Sep. 2012.

[17] A. Balogun, O. Ojo, and F. Okafor, "Decoupled direct control of natural and power variables of doubly fed induction generator for extended wind speed range using feedback linearization," *IEEE Trans. Emerg. Sel. Topics Power Electron.*, vol. 1, no. 4, pp. 226–237, Dec. 2013.
[18] T. K. Boukas and T. G. Habetler, "High-performance induction motor speed control using exact feedback linearization with state and state derivative feedback," *IEEE Trans. Power Electron.*, vol. 19, no. 4, pp. 1022–1028, Jul. 2004.
[19] D.-C. Lee, G.-M. Lee, and K.-D. Lee, "DC-bus voltage control of three-phase AC/DC PWM converters using feedback linearization," *IEEE Trans. Ind. Appl.*, vol. 36, no. 3, pp. 826–833, May/Jun. 2000.
[20] S. Yang, P. Wang, and Y. Tang, "Feedback linearization-based current control strategy for modular multilevel converters," *IEEE Trans. Power Electron.*, vol. 33, no. 1, pp. 161–174, Jan. 2018.
[21] Z. Li, Q. Hao, F. Gao, L. Wu, and M. Guan, "Nonlinear decoupling control of two-terminal MMC-HVdc based on feedback linearization," *IEEE Trans. Power Del.*, vol. 34, no. 1, pp. 376–386, Feb. 2019.
[22] Y. Gui, X. Wang, H. Wu, and F. Blaabjerg, "Voltage-modulated direct power control for a weak grid-connected voltage source inverters," *IEEE Trans. Power Electron.*, vol. 34, no. 11, pp. 11 383–11 395, Nov. 2019.
[23] Y. Zou, J. Qin, L. Zhang, and Z. Zhang, "Novel control approach for modular multilevel converter based on alpha beta 0 reference frame without PLL," in *Proc. IEEE Energy Convers. Congr. Expo.*, 2018, pp. 3044–3049.
[24] D. Roiu, R. I. Bojoi, L. R. Limongi, and A. Tenconi, "New stationary frame control scheme for three-phase PWM rectifiers under unbalanced voltage dips conditions," *IEEE Trans. Ind. Appl.*, vol. 46, no. 1, pp. 268–277, Jan./Feb. 2010.
[25] Q.-C. Zhong and G. Weiss, "Synchronverters: Inverters that MIMIC synchronous generators," *IEEE Trans. Ind. Electron.*, vol. 58, no. 4, pp. 1259–1267, Apr. 2011.
[26] H. Wu *et al.*, "Small-signal modeling and parameters design for virtual synchronous generators," *IEEE Trans. Ind. Electron.*, vol. 63, no. 7, pp. 4292–4303, Jul. 2016.
[27] L. Zhang, L. Harnefors, and H.-P. Nee, "Power-synchronization control of grid-connected voltage-source converters," *IEEE Trans. Power Syst.*, vol. 25, no. 2, pp. 809–820, May 2010.
[28] A. Jamshidifar and D. Jovcic, "Small-signal dynamic DQ model of modular multilevel converter for system studies," *IEEE Trans. Power Del.*, vol. 31, no. 1, pp. 191–199, Feb. 2016.
[29] Y. Zou, J. Qin, L. Zhang, and J. Yu, "Inequality constraint based method for fast estimation of droop-slope stability regions for MMC-based MTDC systems," *IEEE Trans. Power Del.*, to be published, 2021, doi: 10.1109/TPWRD.2020.3048307.
[30] K. Ilves, A. Antonopoulos, S. Norrga, and H.-P. Nee, "Steady-state analysis of interaction between harmonic components of arm and line quantities of modular multilevel converters," *IEEE Trans. Power Electron.*, vol. 27, no. 1, pp. 57–68, Jan. 2012.
[31] C. Kravaris and M. Soroush, "Synthesis of multivariable nonlinear controllers by input/output linearization," *AIChE J.*, vol. 36, no. 2, pp. 249–264, 1990.
[32] B. Zhao, Q. Song, J. Li, Y. Wang, and W. Liu, "Modular multilevel high-frequency-link DC transformer based on dual active phase-shift principle for medium-voltage DC power distribution application," *IEEE Trans. Power Electron.*, vol. 32, no. 3, pp. 1779–1791, Mar. 2017.
[33] L. Zhang, J. Qin, Y. Zou, Q. Duan, and W. Sheng, "Analysis of capacitor charging characteristics and low-frequency ripple mitigation by two new voltage-balancing strategies for MMC-based solid-state transformers," *IEEE Trans. Power Electron.*, vol. 36, no. 1, pp. 1004–1017, Jan. 2021.

Yuntao Zou (Student Member, IEEE) received the B.S. degree from Northwest A&F University, Yangling, China, in 2014, and the M.Eng. degree from Xi'an Jiaotong University, Xi'an, China, in 2017, both in electrical engineering. He is currently working toward the Ph.D. degree in electrical engineering with Arizona State University, Tempe, AZ, USA.

His research interests include system modeling and control of MMC and MMC-based MTDC systems, dynamic performance and stability of MTDC systems, and integration and control of renewable energy sources.

Lei Zhang (Member, IEEE) received the B.Eng. degree from the Shandong University of Science and Technology, Qingdao, China, in 2012, the M.Eng. degree from Shandong University, Jinan, China, in 2015, and the Ph.D. degree from the Arizona State University, Tempe, AZ, USA, in 2020, all in electrical engineering.

From 2015 to 2016, he was with the School of Electrical and Electronic Engineering, Nanyang Technological University, where he worked as a Research Associate. His research interests include the modular multilevel converters (MMC), energy storage system, and hybrid ac–dc microgrid.

Jiangchao Qin (Senior Member, IEEE) received the Ph.D. degree in electrical engineering from Purdue University, West Lafayette, IN, USA, in 2014.

He is currently as Associate Professor with the Department of Electrical Engineering, Shanghai Jiao Tong University, Shanghai, China. His research interests include power electronics, applications of power electronics in power systems, and electric machines and drives.

Wanxing Sheng (Senior Member, IEEE) was born in China in 1965. He received the Ph.D. degree in electronic engineering from Xian Jiaotong University, Xi'an, China, in 1995.

Since 1997, he has been a Full Professor with China Electric Power Research Institute, Beijing, China, where he is currently the Head of the Department of Power Distribution. He is also a Leader of intelligent distribution system and an excellent expert of the State Grid Corporation, China, Beijing.

Qing Duan (Member, IEEE) received the M.S. degree from the Huazhong University of Science and Technology, Wuhan, China, in 2004, and the Ph.D. degree from Shandong University, Jinan, China, in 2010.

He was a Visiting Scholar with Arizona State University, Tempe, AZ, USA, from 2017 to 2018. He is currently a Senior Engineer with the Institute of Power Distribution, China Electric Power Research Institute, Beijing, China. His research interests include power electronics technologies, power distribution grid systems, and the energy Internet.